# Large Deformations in Oriented Polymer Glasses: Experimental Study and a New Glass-Melt Constitutive Model

**DAVIDE S. A. DE FOCATIIS,[1][†] JOHN EMBERY,[2][‡] C. PAUL BUCKLEY[1]**

[1]Department of Engineering Science, University of Oxford, United Kingdom

[2]School of Physics and Astronomy, University of Leeds, United Kingdom

**ABSTRACT:** An experimental study was made of the effects of prior molecular orientation on large tensile deformations of polystyrene in the glassy state. A new hybrid glass-melt constitutive model is proposed for describing and understanding the results, achieved by parallel coupling of the ROLIEPOLY molecularly-based melt model with a model previously proposed for polymer glasses. Monodisperse and polydisperse grades of polystyrene are considered. Comparisons between experimental results and simulations illustrate that the model captures characteristic features of both the melt and glassy states. Polystyrene was stretched in the melt state and quenched to below $T_g$, and then tensile tested parallel to the orientation direction near the glass transition. The degree of strain-hardening was observed to increase with increasing prior stretch of molecules within their entanglement tubes, as predicted by the constitutive model. This was explored for varying temperature of stretching, degree of stretching, and dwell time before quenching. The model in its current form, however, lacks awareness of processes of subentanglement chain orientation. Therefore, it underpredicts the orientation-direction strain hardening and yield stress increase, when stretching occurs at the lowest temperatures and shortest times, where it is dominated by subentanglement orientation. © 2010 Wiley Periodicals, Inc. J Polym Sci Part B: Polym Phys 48: 1449–1463, 2010

**KEYWORDS:** constitutive model; glass transition; orientation; polystyrene; rheology; ROLIEPOLY; simulations

## INTRODUCTION

As demonstrated by a wide range of polymer products, molecular orientation is one of the fundamental parameters that determine the mechanical response of a melt processed, thermoplastic polymer.[1] The degree of orientation present within a particular product is a complex function of its rheology and the process parameters employed. The rheological behavior itself is intrinsically linked to the molecular weight and its distribution, and the chain architecture, as well as the presence of any additives. Consequently, as industrial polymer processing engineers have long known, mechanical properties of practical importance such as Young's modulus, yield stress, and fracture toughness in any given direction are highly sensitive to the grade of polymer employed and the flow history encountered during processing.[2–9] Therefore, it is of great practical interest to understand better the development of frozen-in molecular orientation during melt processing, and the relationships between this orientation and resulting solid-state properties. In particular, there is an engineering need to achieve a predictive capability, for use in optimizing polymer products.

Progress toward predicting the large deformation solid-state performance of polymer products with process-induced molecular orientation requires a constitutive model applicable to both solid and melt states. In the melt, molecules are oriented by the flow and stretched within their entanglement constraint tubes. Any subsequent solid-state deformation leads to a continued evolution of orientation and stretch, in parallel with short-range effects such as segmental diffusion and structural evolution. A model is required that is sufficiently comprehensive to capture this range of behavior. Moreover, a desirable feature of such a model would be the incorporation of information about the chemical structure of the polymer, such as molecular length and architecture. This would enable the concurrent design of compatible materials and processes to produce optimized products with the desired properties.

A basis for finite deformation constitutive models of amorphous polymeric solids is provided by the one-dimensional model of Haward and Thackray.[10] Two contributions are ascribed to the free energy and hence the stress, arising from (a) perturbation of interatomic potentials, relaxed by isotropic segmental flow, and (b) perturbation of conformational entropy of the entangled molecular network, represented in the glassy state as a crosslinked network. These ideas have been incorporated into fully three-dimensional

constitutive models by several researchers. Examples of studies that employed this kind of description include those of Buckley and coworkers,[11–13] Boyce and coworkers,[14,15] and Govaert and coworkers.[16–18] A notable feature of such a model is that all the strain-hardening observed experimentally at large deformations is attributed to the nonlinear elasticity of contribution (b) above. Various free energy functions originating from rubber elasticity theory have been employed to capture this. Although such models have proved useful phenomenological tools for describing the constitutive behavior of initially isotropic polymers below $T_g$, at constant temperature and strain-rate, they all exhibit important inconsistencies with the underlying polymer physics. For example, the apparent crosslink density required to fit the experimental observations is orders of magnitudes larger than the entanglement density evaluated from melt rheology.[19] In addition, the strain-hardening is rate-sensitive,[20] inconsistent with the elasticity of a crosslinked network, and reduces with increase in temperature,[18,21] inconsistent with entropic elasticity. Moreover, Govaert and Tervoort also found that for polycarbonate, the strain hardening increased with increasing molecular weight.[18] This is in contrast with the widely held view that the entanglement density is, at a given temperature, an intrinsic property of the polymer itself and does not depend on molecular weight.

For all these reasons, there is growing recognition that the form of constitutive model described above is inadequate to capture large deformations in polymer glasses over a wide range of rate and temperature. There may be two physically separate processes causing this. (I) Near and above the glass transition, the conformational entropy of the entanglement network begins to relax on the experimental time-scale, by molecular diffusion within the tube. Therefore, the entropic stress contribution from the entanglement network is expected to become elastoviscous, and to exhibit the forms of dependence on rate, temperature, and molecular weight observed. (II) Deep in the glassy state, where tube diffusion is expected to be frozen, the rate and temperature dependence of the strain hardening may indicate that it has been mis-attributed to the entanglement network. If most of the strain-hardening comes instead from strain-dependence of the resistance to segmental flow, the experimental observations can be explained.[20–22]

Since this work requires a constitutive model that spans both the melt and glassy states, we focus attention on incorporating process I identified above into the constitutive model of a polymer glass. Several previous authors have addressed this question and have modified constitutive models for polymer glasses by incorporating a representation of the relaxation of conformational entropy. In all cases to date, the approach adopted was phenomenological, aimed at achieving a good match to experiment, to provide an effective capability for modeling highly elastic flows just above the glass transition encountered, for example in thermoforming and stretch-blow molding processes. Examples of this approach are the studies of poly(methyl methacrylate) by Dooling et al.[23] and more recently by Dupaix and coworkers,[24] and of poly(ethylene terephthalate) by Buckley and coworkers[25] and Boyce and co-

workers.[26] Useful empirical fits to data can be achieved in this manner, but the approach has two major disadvantages. First, the constitutive description does not extend deep into the melt, to provide a unified constitutive model that also captures melt rheology further upstream in the flow history that may still impact on eventual solid state properties. Second, phenomenological models lack molecular awareness: they cannot predict the consequences of changing molecular structure or chain length. Therefore, they preclude a genuinely holistic design of polymer, processing and part that is the eventual goal of modeling.

Meanwhile, in a separate development, there has been much recent progress in formulating molecularly aware rheological models for polymer melts. Deformation of monodisperse linear polymer melts, where the interaction between stretching and relaxation of the entanglement network dominates the behavior, has been successfully modeled by McLeish and coworkers using a full, molecularly based, linear constitutive theory of polymer melts.[27] The ROuse model for LInear Entangled POLYmers, known as the ROLIEPOLY model, was derived subsequently as a mathematical simplification of the full linear theory, more amenable to large-scale computation.[28] This constitutive equation was implemented in a Lagrangian flow solver[29] and has been deployed with great success, to accurately predict the flow of melts in complex geometries.[30–32] In view of the success of this approach deep in the melt state, this work explores its ability to capture the rheology in highly elastic flows nearer to the glass transition, by providing a molecularly based description of the process I referred to above.

Thus, a new hybrid glass-melt constitutive model is proposed here that aims to capture deformation in both the glassy and melt states. The model consists of a set of ROLIEPOLY equations that govern the conformational entropy elasticity of the polymer and its relaxation by tube diffusion in the melt, and a multi-mode glassy constitutive model for deformation of PS developed previously in the Oxford laboratory.[13] The combined model is parameterized through the full linear viscoelastic spectrum.

The model was used in interpreting the results from an experimental study of the constitutive responses of three grades of atactic polystyrene (PS), including the effects of molecular orientation induced by stretching above the glass transition. The linear melt rheology of the three PS grades was characterized to extract the relevant material properties to be used in the POLIEPOLY part of the model. Much of the characterization of the glassy part of the model was based on the previous experimental results of Wu and Buckley.[13] The two monodisperse grades and one polydisperse grade of amorphous PS were oriented at a range of temperatures in the melt. Initially isotropic specimens were stretched uniaxially at different temperatures above $T_g$, to different draw ratios, followed by different durations of stress-relaxation before quenching to below $T_g$. The conditions used were chosen so as to explore a wide range of degrees of molecular orientation. The resulting specimens were then drawn in tension below $T_g$, parallel to the original stretch direction, to

| | Code | $M_w$ (g/mol) | PDI | Architecture | $T_g$ (°C) |
|---|---|---|---|---|---|
| Monodisperse | AF | 262,000 | 1.05 | linear | 105.7 ± 1.3 |
| Monodisperse | AG | 518,000 | 1.15 | linear | 107.5 ± 0.9 |
| Polydisperse | R | 216,000 | 2.54 | linear | 104.7 ± 0.7 |

measure the effects of melt state orientation on their constitutive response in the glassy state.

## EXPERIMENTAL

### Materials

The materials used in this study were two samples of monodisperse linear atactic PS (PDI $= M_w/M_n < 1.15$) and one sample of polydisperse linear atactic PS (Dow GP680E base polymer with no additives). The codes used to refer to the materials in this article are consistent with previous publications on these polymers.[33,34] Monodisperse materials AF and AG were synthesized by living anionic polymerization at Durham and were provided by Dr. Lian Hutchings of the University of Durham, whereas polydisperse material R was provided by the Dow Chemical Company. Molar mass measurements were kindly performed by Dr. Hutchings by size exclusion chromatography (SEC) on a Viscotek TDA 302 machine with refractive index, viscosity, and light scattering detectors, and results are given in Table 1.

### Differential Scanning Calorimetry

The glass transition of all three polystyrene samples was studied using differential scanning calorimetry (DSC) with a TA DSC Q10 instrument. DSC runs consisting of a heating ramp to 160 °C, a cooling ramp to 60 °C, and a reheating ramp to 160 °C, all conducted at 10 °C min$^{-1}$, were repeated three times for each material. $T_g$ was identified for each run using the TA Universal Analysis 2000 Version 4.3A software's onset-end intercept method. Average values of $T_g$ for each material are given in Table 1.

### Rheometry

Linear melt rheology in shear was analyzed for all materials using an Ares L2 rheometer with 10 mm parallel plates. A temperature range of between 130 °C and 230 °C was used. The curves of $G'$ and $G''$ versus log(frequency) were shifted using time–temperature superposition to provide a single master curve for each polymer at a reference temperature of 170 °C. The master curves are shown in Figure 1.

Nonlinear rheology was analyzed for all materials using an Ares L2 rheometer with 10 mm diameter cone and plate in transient shear, and with a Sentmanat extensional rheometer fixture[36] in extension. A temperature of 170 °C was used, with applied strain rates ranging from 0.01 s$^{-1}$ to 6 s$^{-1}$ in shear and 0.06 s$^{-1}$ to 10 s$^{-1}$ in extension. Measurements of viscosity are plotted against time in Figure 2.

### Production of Isotropic Specimens

The starting specimens used in this work were all in the form of isotropic bars of PS, formed by compression molding. Owing to the limited quantities of the monodisperse materials available, and the brittle nature of polystyrene, a technique for near net shape production of small parallelepipedic bars was employed. The aim was to minimize material waste and to keep stress applied to specimens during their removal from the mold to a minimum.

A steel mold consisting of upper and lower steel plates, with a central steel multiple cavity plate 0.5 mm in thickness, was used to mold rectangular bars in a hand-operated hydraulic press with heated platens. The central steel cavity plate ensures accurate location of the removable steel inserts, which define the specimen geometry and allow for easy removal of the specimens after molding. Fresh sheets of disposable 0.15 mm thick soft temper 1200 aluminum foil obtained from Multifoil Ltd were sandwiched between the top steel plate and the cavity plate, and the bottom steel plate and the cavity plate to provide a repeatable surface texture on the molded specimens. The foil sheets, the mold cavity plate, and the inserts were lightly sprayed with a dry PTFE mold release aerosol, before each molding operation.
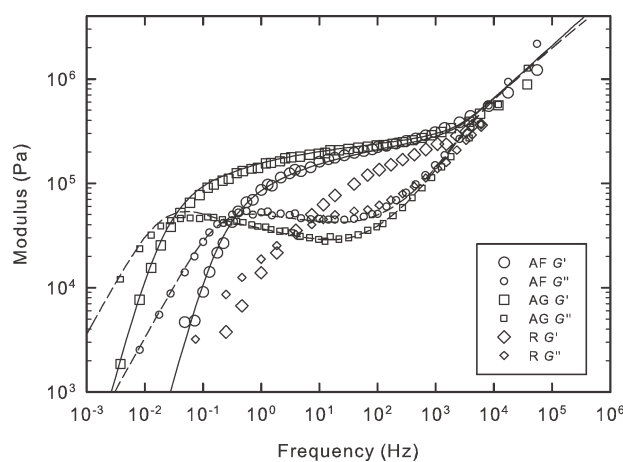


FIGURE 1 Storage moduli ($G'$—large symbols) and loss moduli ($G''$—small symbols) obtained from linear viscoelastic shear melt rheology, shifted to 170 °C using time–temperature superposition, for the three polymers used in this study. Also shown are the moduli obtained from of the Likhtman-McLeish quantitative theory[35] used to obtain the material parameters $G_e$, $M_e$, and $\tau_e$ from the monodisperse materials AF and AG ($G'$—solid lines and $G''$—dashed lines).
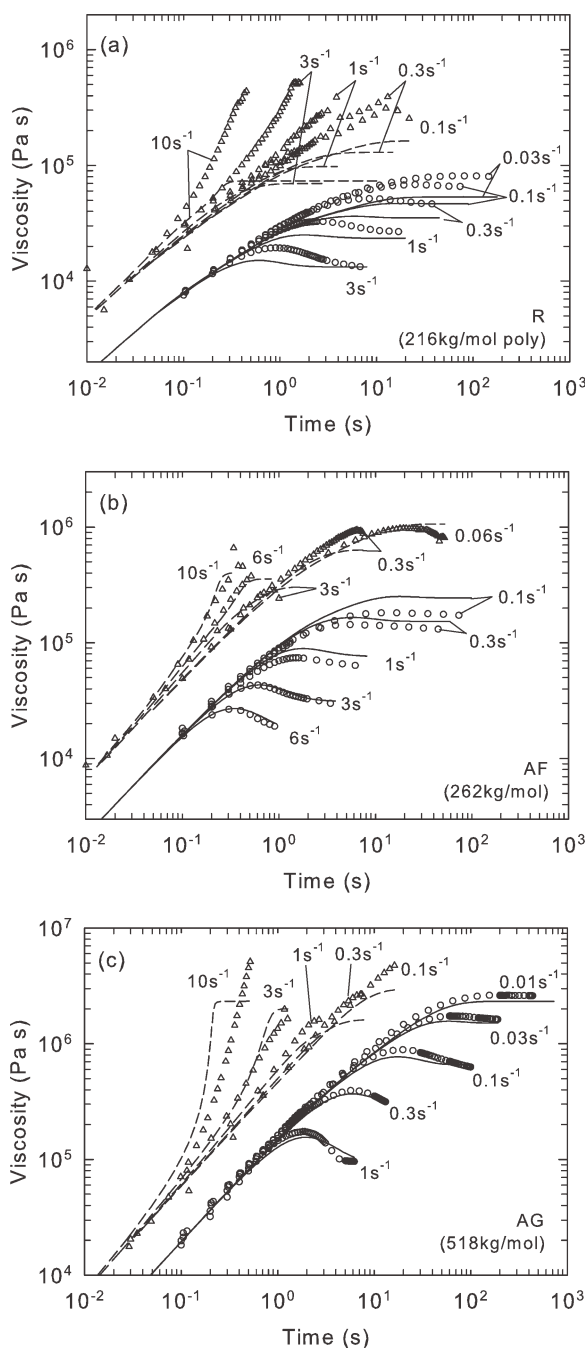
**FIGURE 2** Transient shear and extensional viscosity measured at 170 °C for: (a) polymer R at a range of rates from 0.03 s$^{-1}$ to 3 s$^{-1}$ in shear, and 0.1 s$^{-1}$ to 10 s$^{-1}$ in extension; (b) polymer AF at a range of rates from 0. 1 s$^{-1}$ to 6 s$^{-1}$ in shear, and 0.06 s$^{-1}$ to 10 s$^{-1}$ in extension; (c) polymer AG at a range of rates from 0.01 s$^{-1}$ to 1 s$^{-1}$ in shear, and 0.1 s$^{-1}$ to 10 s$^{-1}$ in extension. Also shown are simulations from the constitutive model.

Each cavity of the mold was then filled with a small excess of polymer before placing the mold between preheated press platens.

The mold reached the molding temperature of 170 °C in ~10 min, during which time the platens were slowly closed.

The clamping force was then cycled manually for a period of 5 min to dislodge any trapped air bubbles. The mold was held at 170 °C at moderate pressure for a further 10 min, and then cooled to room temperature at a rate of ca 15 °C/min by flushing cold water through cooling channels in the press platens. The mold was removed from the press when the temperature reached 70 °C. The temperature during a typical molding cycle, monitored with an embedded thermocouple can be found in our previous report.[33] The moldings were verified as optically isotropic. Small amounts of flash were removed from the sides of the specimens after molding using fine grades of abrasive paper. Typical specimens produced with this mold have dimensions of 80 mm × 6 mm × 0.5 mm, although other geometries are possible.

### Production of Oriented Specimens

Molecular orientation was introduced by melt drawing the prismatic bars of PS in an Instron 4204 testing machine fitted with an environmental chamber at a range of temperatures $T$ around and above $T_g$, at a constant crosshead velocity corresponding to a nominal strain rate of 0.02 s$^{-1}$. The bars were gripped using pneumatic grippers, with the lower grip actuated after 12 min, when the oven temperature settled. They were then stretched uniaxially to a range of draw ratios $\lambda$ between 2 and 4, and then quench cooled to below $T_g$, using a cold spray applied at the end of the drawing process, giving an initial cooling rate of ~15 °C/s. In some experiments, a dwell time $t$ was allowed at the end of stretching, for isothermal stress-relaxation to occur at constant grip displacement, before quenching. Strain was measured using an Instron noncontact video extensometer tracking black marks applied on the sample using a water-based ink. Temperature was monitored throughout the experiments using two thermocouples positioned close to the bars. The tensile load was recorded throughout the orientation and dwell process. The oriented bars were then stored at room temperature before redrawing.

To explore systematically the separate roles of the three variables $T$, $t$, and $\lambda$, three procedures were followed:

### Procedure I, Varying T

The monodisperse materials AF and AG and the commercial polydisperse material R were hot-drawn at a range of temperatures $T$ from 105 °C to 135 °C, to a fixed draw ratio $\lambda = 3$ at a constant nominal strain rate 0.02 s$^{-1}$, and immediately quenched using the cold spray.

### Procedure II, Varying t

The polydisperse material R was hot-drawn at a temperature $T = 105$ °C, to a fixed draw ratio $\lambda = 3$ at a constant nominal strain rate 0.02 s$^{-1}$, and a range of dwell times $t$ from 1 s to 3000 s were allowed before quenching, to allow relaxation to take place at the draw temperature.

### Procedure III, Varying λ

The monodisperse materials AF and AG and polydisperse material R were drawn to a range of draw ratios $\lambda$ from 2 to 4 at a constant nominal strain rate 0.02 s$^{-1}$ at a temperature

**TABLE 2** Summary of the Test Procedures for Preparing Uniaxially Oriented Specimens

| Procedure | Strain Rate ($s^{-1}$) | Draw Ratio $\lambda$ | Temperature $T$ | Dwell Time $t$ at End of Test | Materials Used |
|---|---|---|---|---|---|
| I | 0.02 | 3 | **105 °C–135 °C** | None | **AF, AG, R** |
| II | 0.02 | 3 | 105 °C | **1–3000 s** | R |
| III | 0.02 | **2-4** | 115 °C | 300 s | **AF, AG, R** |

In each case, the parameters used as variables are highlighted in bold.

$T = 115$ °C. A dwell time $t$ of 300s was allowed before quenching.

A summary of the procedures is presented in Table 2, with the parameters used as variables highlighted in bold.

The production of oriented specimens was challenging for a variety of reasons: in general, the limited availability of materials precluded repetitions of the tests; at low draw temperatures, the specimens were prone to either brittle fracture or to the formation of inhomogeneous deformation zones, or necks; at high draw temperatures, the specimens were prone to failure at the grips. The range of temperatures and dwell times reported here indicate the range in which uniform specimens were able to be both produced and retested in the glassy state. In the cases where inhomogeneous deformation was visible, the specimens have been excluded from the analysis.

### Sub-$T_g$ Testing of Oriented Specimens

All the oriented bars were tested in uniaxial tension in the same Instron testing machine as used for the orientation process, with the environmental chamber at a fixed temperature $T_r = 96$ °C $\pm$ 1 °C, and a constant crosshead velocity corresponding to a nominal strain rate of 0.001 $s^{-1}$. This temperature was chosen in the narrow temperature window between $T_g$ and the temperature at which some of the bars became too brittle to test. The oriented bars were gripped in the same manner as for the orientation process. They were tested until failure, or until visible necking ensued. In general, necking was suppressed in the oriented bars, occurring infrequently and only in the bars preoriented at the highest temperatures. Strain was measured using an Instron noncontact video extensometer. Because of the tendency of some bars to stress-whiten at large extensions, the oriented bars were painted black using a water-based ink and silver reflective marks applied over the black ink were tracked by the extensometer.

Figure 3(a–c) illustrates measured stresses as a function of nominal strains for the bars oriented according to Procedure I, for the materials AF, AG, and R. The plots are on identical axes to illustrate the differences across the materials on the glassy response. Figure 4 illustrates measured stresses as a function of nominal strains for the bars of polymer R oriented according to Procedure II, drawing at 105 °C and varying the dwell time $t$. Figure 5(a–c) illustrates measured stresses as a function of nominal strains for the bars oriented according to Procedure III, varying the draw ratio during hot-drawing. Again the plots are on identical axes to illustrate the effects of the differences in draw ratio on the glassy response.

### CONSTITUTIVE MODEL

**Basis**

The following is a fully three-dimensional constitutive model for amorphous polymers, combining the Oxford Glass-Rubber (GR) constitutive model proposed first for irrotational displacement fields[11] and later for generic displacement fields,[13,23] with the ROLIEPOLY constitutive equations of Likhtman et al.[28] The combined model is based on the assumption that in a deformed amorphous polymer, free energy is stored through (a) perturbation of interatomic potentials, or bond-stretching, and through (b) changes in the supra-entanglement molecular conformational entropy, and that these two contributions to the free energy are additive.

The constitutive model describes the material response to a deformation gradient tensor $\boldsymbol{F}$ in terms of the Cauchy stress tensor $\boldsymbol{\sigma}$. $\boldsymbol{F}$ is separated into volumetric and deviatoric parts, given respectively, by the following:

$$J = \det \boldsymbol{F} \text{ and } \overline{\boldsymbol{F}} = J^{-\frac{1}{3}}\boldsymbol{F}. \tag{1}$$

The stress tensor $\boldsymbol{\sigma}$ is similarly separated into volumetric $\sigma_m$ and deviatoric $\boldsymbol{S}$ parts, given by the following:

$$\sigma_m = K \ln J = \frac{1}{3}\text{tr}\,\boldsymbol{\sigma} \text{ and } \boldsymbol{S} = \boldsymbol{\sigma} - \sigma_m\boldsymbol{I} \tag{2}$$

where $K$ is the bulk modulus.

From the assumption of additivity of the bond-stretching and conformational free energies, the deviatoric stress can be expressed as the sum of (a) a bond-stretching stress $\boldsymbol{S}^b$ and (b) a conformational stress $\boldsymbol{S}^c$

$$\boldsymbol{S} = \boldsymbol{S}^b + \boldsymbol{S}^c. \tag{3}$$

**Bond-Stretching Stress**

The bond-stretching part of the model mirrors our previous approach in the modeling of glassy polymers and only a brief treatment will be given here. The reader is advised to consult previous papers[11–13,23] for a more detailed discussion. The deviatoric rate of deformation tensor $\overline{\boldsymbol{D}}$ can be computed from the isochoric velocity gradient tensor $\overline{\boldsymbol{L}}$, given by the following:

$$\overline{\boldsymbol{L}} = \overline{\boldsymbol{F}} \cdot \overline{\boldsymbol{F}}^{-1}, \quad \overline{\boldsymbol{D}} = \frac{\overline{\boldsymbol{L}} + \overline{\boldsymbol{L}}^T}{2} \tag{4}$$

$$\overline{\boldsymbol{D}} = \frac{\hat{\boldsymbol{S}}_j^{\mathrm{b}}}{2G_{\mathrm{b}}} + \frac{\boldsymbol{S}_j^{\mathrm{b}}}{2G_{\mathrm{b}}\tau_j}, \quad \boldsymbol{S}^{\mathrm{b}} = \sum_{j=1}^{M} v_j \boldsymbol{S}_j^{\mathrm{b}}, \quad \sum_{j=1}^{M} v_j = 1 \qquad (5)$$

where $\hat{\boldsymbol{S}}_j^{\mathrm{b}}$ is an objective, corotational, rate of change of the $j$th bond-stretching stress $\boldsymbol{S}_j^{\mathrm{b}}$ (implemented as the Jaumann rate), $G_{\mathrm{b}}$ is the bond-stretching shear modulus, $v_j$ represents the relative weighting of each mode, and $\tau_j$ is the relaxation time associated with the $j$th glassy mode. The glassy relaxation time is referred back to an unstressed relaxation time $\tau_{j,0}^*$ at a reference temperature $T^*$ and structural state $T_{\mathrm{f}}^*$ through shift factors for temperature, structure, and stress, respectively.

$$\tau_j = a_{\mathrm{T}} a_{\mathrm{s}} a_{\boldsymbol{\sigma},j} \tau_{j,0}^* \qquad (6)$$

where

$$\begin{aligned} a_{\mathrm{T}} &= \exp\left[\frac{\Delta H}{R}\left(\frac{1}{T} - \frac{1}{T^*}\right)\right] \\ a_{\mathrm{s}} &= \exp\left[\frac{C}{T_{\mathrm{f}} - T_\infty} - \frac{C}{T_{\mathrm{f}}^* - T_\infty}\right] \\ a_{\boldsymbol{\sigma}} &= \frac{V_{\mathrm{s}} \tau_{\mathrm{oct},j}^{\mathrm{b}}}{2RT} \frac{\exp\left(-\frac{V_{\mathrm{p}} \sigma_{\mathrm{m}}}{RT}\right)}{\sinh\left(\frac{V_{\mathrm{s}} \tau_{\mathrm{oct},j}^{\mathrm{b}}}{2RT}\right)} \end{aligned} \qquad (7)$$

The material constants are as employed by Wu and Buckley:[13] $\Delta H$ is the activation enthalpy, $T_\infty$ is the Vogel temperature, $C$ is the Cohen Turnbull constant, $V_{\mathrm{s}}$ and $V_{\mathrm{p}}$ are the shear and pressure activation volumes, and $\tau_{\mathrm{oct},j}^{\mathrm{b}}$ is the octahedral shear stress acting on the $j$th mode.

In this article, the structural evolution visible during mechanical deformation below $T_{\mathrm{g}}$ as a yield peak and subsequent strain-softening, is modeled through a semi-empirical expression connecting the evolution of $T_{\mathrm{f}}$ with viscoplastic strain[12]
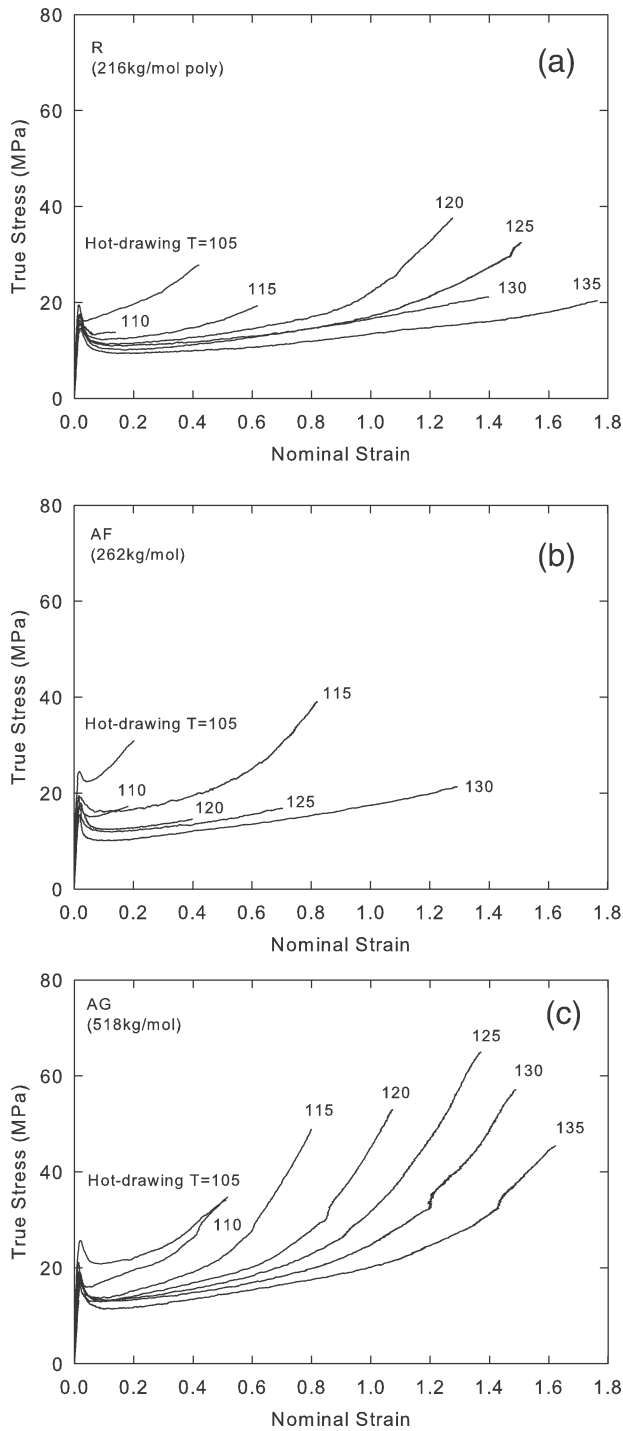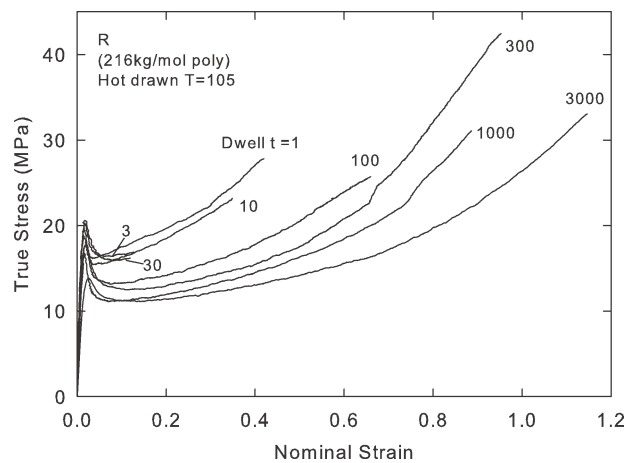


FIGURE 3 True stress plotted against nominal strain measured during glassy-state uniaxial testing ($T_{\mathrm{r}} = 96$ °C, $\dot{\varepsilon} = 0.001\,\mathrm{s}^{-1}$) of bars melt stretched according to procedure I, at a range of temperatures $T = 105$ °C–135 °C followed by immediate quenching, for materials R (a), AF (b), and AG (c).



FIGURE 4 True stress plotted against nominal strain measured during glassy-state uniaxial testing ($T_{\mathrm{r}} = 96$ °C, $\dot{\varepsilon} = 0.001\,\mathrm{s}^{-1}$) of bars of polymer R melt stretched according to procedure II, at temperature $T = 105$ °C followed by a range of dwell times $t$ (seconds) before quenching.

where $\dot{\overline{\boldsymbol{F}}}$ is the time derivative of $\overline{\boldsymbol{F}}$. The deviatoric rate of deformation $\overline{\boldsymbol{D}}$ is the sum of a linear elastic bond stretching part, and a part from the viscous flow of molecular segments. Following Wu and Buckley,[13] we use a multimode discrete spectrum of $M$ modes
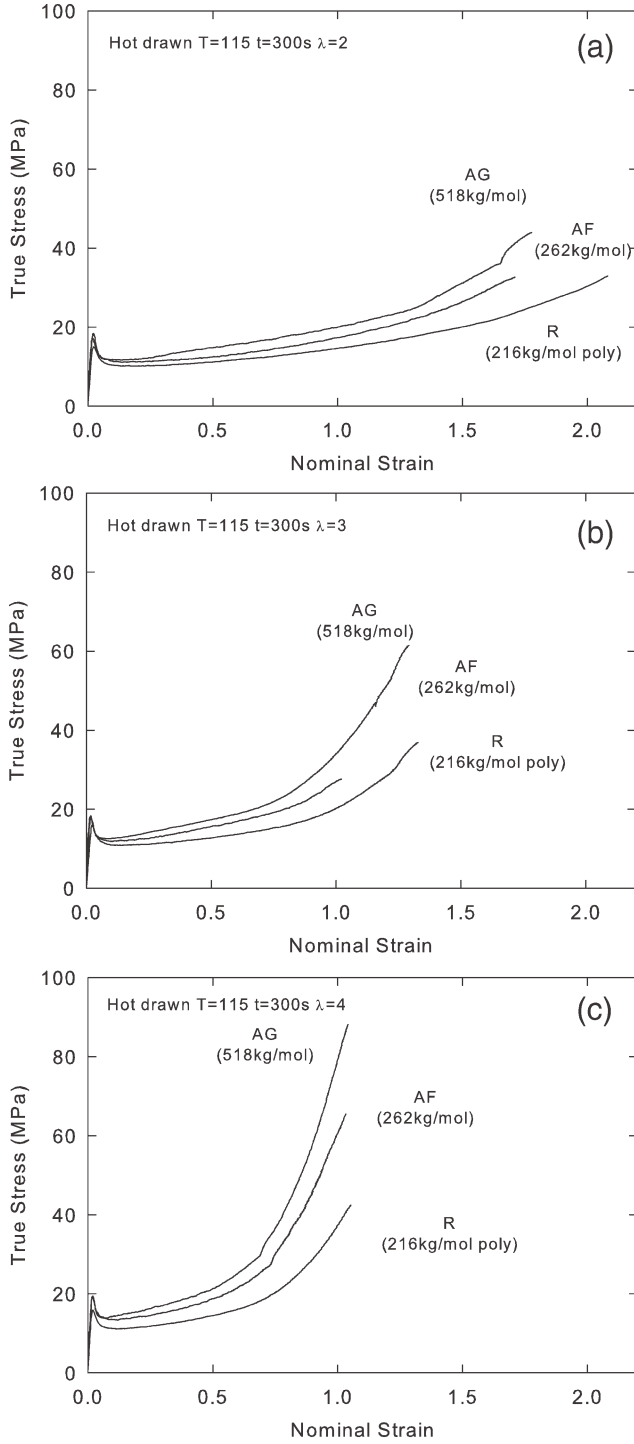
**FIGURE 5** True stress plotted against nominal strain measured during glassy-state uniaxial testing ($T_r = 96\,°C$, $\dot{\varepsilon} = 0.001\,s^{-1}$) of bars melt stretched according to procedure III, at a temperature of $T = 115\,°C$ followed by a dwell time of 300 s before quenching, for draw ratios $\lambda = 2$ (a), $\lambda = 3$ (b), and $\lambda = 4$ (c).

$$T_f = T_{f,0} + \Delta T_f \left[ 1 - \exp\left( -\frac{\bar{\varepsilon}^v}{\varepsilon_0^v} \right) \right] \tag{8}$$

where $T_{f,0}$ and $\Delta T_f$ are the initial fictive temperature and the increase in fictive temperature due to plastic strain, $\varepsilon_0^v$ is a material parameter, and $\bar{\varepsilon}^v$ is the equivalent viscoplastic strain invariant. Equation 8 neglects the rate dependence of $\Delta T_f$ and $\varepsilon_0^v$ and does not provide for the prediction of $T_{f,0}$ as a consequence of prior thermal history of the glass. If more predictive capability is required, it is necessary to provide a model for the kinetics of evolution of $T_f$ for example as suggested by Figiel et al.[37]

**Conformational Stress**

The conformational stress is computed via the ROLIEPOLY constitutive model, a simplified form of a full microscopic theory of linear entangled polymer melts. The ROLIEPOLY model has also been described in detail previously[28] and only a brief treatment will be given here. Since this study explores the applicability of the model to semi-solid states with high degrees of stretch and limited relaxation, it is necessary to employ a version of the ROLIEPOLY equation with finite chain extensibility, kindly provided by Dr D. J. Read of the University of Leeds. In this preliminary study, we do not consider the effects of convective constraint release (i.e., we take $\beta = 0$ in the terms of Likhtman and Graham[28]).

Following Likhtman and Graham,[28] we use a spectrum of $N$ discrete ROLIEPOLY modes to represent the conformational stress and compute a stress in each mode from its corresponding orientation tensor $\boldsymbol{T}_k$. The orientation tensor is governed by the ROLIEPOLY differential equation, modified to allow for finite extensibility

$$\dot{\boldsymbol{T}}_k = \bar{\boldsymbol{L}} \cdot \boldsymbol{T}_k + \boldsymbol{T}_k \cdot \bar{\boldsymbol{L}}^T - \frac{1}{\tau_k^d} \left( \boldsymbol{T}_k - \lambda_k^2 \boldsymbol{I} \right) - \frac{2}{\tau_k^R} \left( \frac{F(\lambda_k) - 1}{\lambda_k} \right) \boldsymbol{T}_k \tag{9}$$

where $\tau_k^R$ and $\tau_k^d$ are the Rouse and reptation times associated with the $k$th mode, and $\lambda_k = \sqrt{\frac{1}{3}\mathrm{tr}(\boldsymbol{T}_k)}$ is the chain stretch associated with the $k$th mode. $F(\lambda_k)$ is given by the following:

$$F(\lambda_k) = \frac{\lambda_{\max}}{3} \left( \frac{\lambda_{\max}^2 - 1}{\lambda_{\max}^2 - 1/3} \right) \mathcal{L}^{-1}\left( \frac{\lambda_k}{\lambda_{\max}} \right) \tag{10}$$

where $\mathcal{L}^{-1}$ is the inverse Langevin function. In the numerical implementation, a Padé approximation to the inverse Langevin function is used.[38] The front factor in eq 10 ensures that $F(1)$ is equal to unity for unstretched modes and that hence no retraction occurs.

After integration of eq 10 to obtain the orientation tensor, the stress in the $k$th mode is calculated from the following:

$$\sigma_k^c = G_e \left[ \left( \frac{F(\lambda_k)}{\lambda_k} \right) \boldsymbol{T}_k - \boldsymbol{I} \right]$$

$$\boldsymbol{S}_k^c = \sigma_k^c - \frac{\boldsymbol{I}}{3} \mathrm{tr}(\sigma_k^c),$$

$$\boldsymbol{S}^c = \sum_{k=1}^{M} \upsilon_k \boldsymbol{S}_k^c, \tag{11}$$

where $\boldsymbol{\sigma}_k^c$ and $\boldsymbol{S}_k^c$ are the full and deviatoric conformational stresses of the $k$th mode,[39] $G_e$ is the entanglement modulus, and $v_k$ represents the relative volume fraction of the $k$th RP mode. The relaxation times are referred back to reference times $\tau_j^{R*}$ and $\tau_j^{d*}$ at temperature $T^*$ and structure $T_f^*$ through shift factors $a_T$ for temperature and $a_s$ for structure, $\tau_j^R = a_T a_s \tau_j^{R*}$ and $\tau_j^d = a_T a_s \tau_j^{d*}$, as defined earlier in eq 7.

To characterize intrinsic material properties of linear PS melts, we used the optimizer Reptate[40] and the microscopic theory of linear polymer melts of Likhtman and McLeish[41] applied to linear rheological data in shear on monodisperse materials AF and AG. The material parameters $G_e$, the entanglement modulus, and $M_e$ and $\tau_e$, the molar mass and Rouse time of one entanglement length, respectively, were established by treating them as variables for a best fit to the theory for monodisperse materials AF and AG, following the approach of Likhtman and McLeish.[35] The parameter $c_v$ was fixed at 1 as in ref. 35.[42] The values of the parameters obtained are as follows: $G_e = 317.9$ kPa, $M_e = 13.14$ kg/mol, and $\tau_e = 0.000697$ s at the reference temperature $T^* = 170$ °C. The longest (whole molecule) mode Rouse time and reptation time were computed following Collis et al.[32]

$$\tau_1^R = Z^2 \tau_e \tag{12}$$

$$\tau_1^d = 3\left(1 - \frac{2.38}{Z^{0.5}} + \frac{4.17}{Z} - \frac{1.55}{Z^{1.5}}\right)Z^3\tau_e \tag{13}$$

where $Z$ represents the number of entanglements. Although the theory was derived for monodisperse linear chains, we examine its applicability to a solid-state model for a typical commercial polydisperse material in this article, and in this case, use $Z = M_w/M_e$.

The finite extensibility (FE) of the chains can be derived from molecular theory using an equivalent Kuhn chain between entanglements, following, for example, Wagner[43] and is given by

$$\lambda_{max} = \sqrt{\frac{n_b}{C_\infty}}\sin(\theta_b/2) \tag{14}$$

where $n_b$ is the number of bonds between entanglements, $C_\infty = 10$ is the characteristic ratio for PS,[44] and $\theta_b$ is the carbon–carbon backbone bond angle, which for PS is 109.28°.[45] Using the value of $M_e$ obtained in this work gives $\lambda_{max} = 4.09$; this value was used in all the simulations reported here.

## Constitutive Model Parameters

To determine a discrete relaxation spectrum fitting the linear viscoelastic data, the procedure employed was as follows. Starting with the mode with the longest relaxation time, $\tau_1^d$, calculated from eqs. 12 and 14, one mode of $\tau^d$ was assigned per decade of time/frequency to cover the range of data of interest, following Likhtman and Graham.[28] The relative weights of the modes were calculated

using a custom-built optimizer written in Matlab to minimize the rms error between the logarithms of the values of $G'$ and $G''$ as obtained by experiment and as calculated from the following:

$$G' = \sum_{i=1}^{M+N-1} G_i \frac{\omega^2\left(\tau_i^d\right)^2}{1 + \omega^2\left(\tau_i^d\right)^2}, \; G'' = \sum_{i=1}^{M+N-1} G_i \frac{\omega\tau_i^d}{1 + \omega^2\left(\tau_i^d\right)^2}. \tag{15}$$

Since the ROLIEPOLY constitutive model is based on entanglement physics, the following condition was imposed:

$$\sum_{k=1}^{N} G_k = G_e. \tag{16}$$

Hence, relative weights $v_k = G_k/G_e$ were attributed to ROLIEPOLY modes until the sum of the modes reached the entanglement modulus $G_e$, and relative weights $v_j = G_j/G_b$ were attributed to the remaining (bond-stretching) modes, until the sum of the modes reached the bond-stretch modulus $G_b = \sum_{j=1}^{M} G_j$. This procedure is illustrated for material AG in Figure 6.

The same procedure was used to obtain discrete spectra for the AF and R materials (not shown). To satisfy eq 16, five RP modes were required for materials R and AF, and six modes for material AG, and one mode occurring at $\omega \approx 1/\tau_e$ was partitioned between RP and glassy modes. A further 12 glassy modes were fitted for all materials.

For each mode, the $\tau_k^d$ values are separated by a decade of time, whereas the corresponding $\tau_k^R$ values are calculated from the value of $Z_k$ corresponding to that mode, by first solving

$$\tau_k^d = 3\left(1 - \frac{2.38}{Z_k^{0.5}} + \frac{4.17}{Z_k} - \frac{1.55}{Z_k^{1.5}}\right)Z_k^3\tau_e \tag{17}$$

for $Z_k$ and then using the corresponding value of $Z_k$ in

$$\tau_k^R = Z_k^2 \tau_e. \tag{18}$$

As an illustrative example, the relaxation times for polymer AG shifted to 120 °C are shown in Table 3. At this temperature, $\tau_e = 10.57$ s.

The reader may find it surprising that a RP mode is present with a value of $Z < 1$. We attach no physical significance to this, but simply use the value of $Z$ as a means of obtaining $\tau_k^R$ associated with the prescribed $\tau_k^d$. Although the spectrum may appear coarse, and some lack of smoothness can be discerned in the calculated plots in Figure 6, when a greater number of modes was used and more detailed spectra were obtained, no significant change could be observed in the calculations of stresses (to follow) at large deformations for the various procedures. For this reason, and with a view to extending the application to a numerical finite element implementation for solid-state deformation, the more computationally efficient representation using only one mode per decade was used throughout this article.
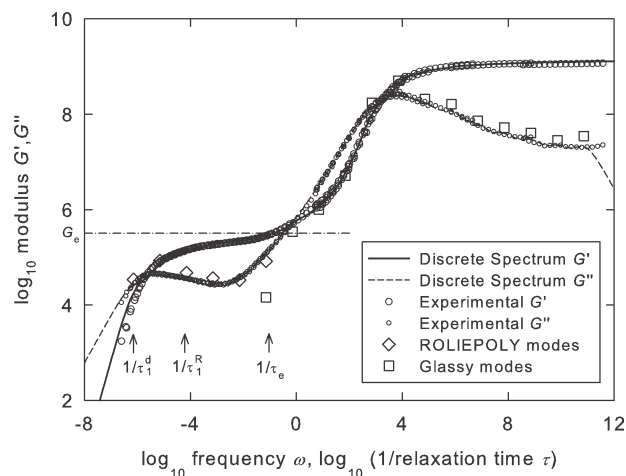
**FIGURE 6** Storage and loss moduli obtained from linear viscoelastic shear rheology (for $\log_{10} \omega < 1$) for polymer AG, and from dynamic mechanical analysis (for $\log_{10} \omega > 1$) for polymer R, from Wu and Buckley,[13] as a function of frequency (squares). Also shown are the storage and loss moduli calculated analytically from the 18-mode spectrum using eq 15 (solid line and dashed line, respectively). The 6 $G_k$ components of the 6-mode RP spectrum are shown as diamonds plotted versus the associated $1/\tau_k^d$. The 13 $G_j$ components of the 13-mode glassy spectrum are shown as squares plotted versus the associated $1/\tau_j$. Also illustrated are the positions of the inverses of the fundamental relaxation times $1/\tau_1^d$, $1/\tau_1^R$, and $1/\tau_e$ and the value of $G_e$.

For the bond-stretch part of the model, where possible the material parameters follow the work on PS of Wu and Buckley.[13] In this work, the thermal history of the redrawn bars involved a quench, differing from that in the earlier work, and the redrawing occurs significantly closer to $T_g$. For this reason, new values of $\Delta H$, $C$, and $T_\infty$ have been found using an optimization routine applied to the shift factor measurements of Wu and Buckley at 110 °C and above. Appropriate values of $T_{f,0}$, $\Delta T_f$, and $\varepsilon_0^v$ have been selected for the present data. The parameters used in the constitutive model simulations are summarized in Table 4. For the RP part of the model, the material parameters used are summarized in Table 5.

## SIMULATION RESULTS

The first test of the constitutive model was to simulate melt rheology in the nonlinear viscoelastic regime and to compare its predictions with experiment. The model simulations are overlaid on the experimental data in Figure 2.

The second test of the constitutive model was to simulate glassy-state compression yield and flow of isotropic specimens of PS at a range of temperatures below $T_g$, for which experimental data and bond-stretch model parameters were provided by Wu and Buckley.[14] Model simulations are overlaid on the experimental data in Figure 7.

The model was then applied to the experimental conditions outlined in Procedures I, II, and III. This involved simulating the following steps:

1. The melt stretching process at a nominal strain rate of $\dot{\varepsilon} = 0.02\,\mathrm{s}^{-1}$ at the prescribed temperature $T$ to the prescribed draw ratio $\lambda$.
2. Holding for the required dwell time $t$ (assumed to be 1 s for cases where no dwell was specifically imposed).
3. A rapid quench, approximated by a decrease in temperature at a constant rate of 15 °C/s down to a temperature of 0 °C.
4. Unloading of the stress (simulated by a rapid contraction at a rate of $\dot{\varepsilon} = -1\,\mathrm{s}^{-1}$; the strain required to achieve unloading is between 0.1% and 0.3% depending on the drawing conditions).
5. Reheating to the glassy-state draw temperature of 96 °C (simulated by a temperature rise at a constant rate of 0.8 °C/s for 120 s).
6. Holding at 96 °C for a time of 600 s (intended to simulate the time taken for the environmental chamber to acclimatize).
7. Uniaxial stretching at 96 °C at a nominal strain rate of $\dot{\varepsilon} = 0.001\lambda\,\mathrm{s}^{-1}$. (intended to simulate the stretching of oriented material at a nominal strain rate of $\dot{\varepsilon} = 0.001\,\mathrm{s}^{-1}$ calculated using its new length after the hot drawing).

As an illustrative example, the full simulation of a bar of polymer AG hot-drawn according to Procedure III at 115 °C, followed by a 300 s dwell time before quenching, unloading, reheating, acclimatizing, and redrawing, is shown in Figure 8.

In the simulation results shown below, only results from the final step (7) are shown. The "nominal strain" during the uniaxial stretching of the oriented material shown in the simulations was computed from the continuous measure of nominal strain $e$ used in all the process as $(e+1)/\lambda - 1$. This was to account for the fact that the measurement of strain in the experiments is computed relative to the new length of the bars after hot drawing and before glassy-state stretching.

Figure 9(a–c) shows model simulations of stresses versus nominal strain for the experimental conditions of Procedure I, for materials R (a), AF (b), and AG (c). The plots are intended to simulate the experimental measurements shown in Figure 3(a–c) and are shown on identical axes to illustrate the differences between the materials and to aid comparison with the data in Figure 3.

Figure 10 shows model simulations of stresses versus nominal strain for the experimental conditions of Procedure II, drawing at 105 °C and varying the dwell time $t$ for material R, and is intended to simulate the experimental measurements shown in Figure 4.

Figure 11(a–c) shows model simulations of stresses versus nominal strain for the experimental conditions of Procedure III, varying the draw ratio during hot-drawing for materials AF, AG, and R to values of $\lambda = 2$(a), $\lambda = 3$(b), and $\lambda = 4$(c).

**TABLE 3** Parameters for the Maxwell Spectrum of Conformational RP Modes and Bond-Stretching Modes Used in Modeling Polymer AG

|  | $k$ | $G_k$ (Pa) | $\tau_k^d$ (s) | $Z_k$ | $\tau_k^R$ (s) | $\upsilon_k$ |
|---|---|---|---|---|---|---|
| RP modes | 1 | 33,910 | 1,400,000 | 39.4 | 16,430.6 | 0.107 |
|  | 2 | 84,900 | 140,000 | 18.9 | 3,774.6 | 0.267 |
|  | 3 | 47,140 | 14,000 | 9.0 | 849.8 | 0.148 |
|  | 4 | 36,490 | 1,400 | 4.1 | 174.9 | 0.115 |
|  | 5 | 33,120 | 140 | 1.7 | 29.8 | 0.104 |
|  | 6 | 82320 | 14 | 0.7 | 4.7 | 0.259 |
|  | $\sum$ | ~318,000 |  |  |  | ~1 |

|  | $j$ | $G_j$ (Pa) | $\tau_j$ (s) | $\upsilon_j$ |
|---|---|---|---|---|
| Glassy modes | 1 | 14,400 | 14 | 0.0000113 |
|  | 2 | 345,200 | 1.4 | 0.000270 |
|  | 3 | 1,004,900 | 0.14 | 0.000787 |
|  | 4 | 5,105,900 | 0.014 | 0.00400 |
|  | 5 | 173,010,200 | 0.0014 | 0.135 |
|  | 6 | 498,729,300 | $1.4 \times 10^{-4}$ | 0.391 |
|  | 7 | 207,406,400 | $1.4 \times 10^{-5}$ | 0.162 |
|  | 8 | 162,745,400 | $1.4 \times 10^{-6}$ | 0.127 |
|  | 9 | 72,773,200 | $1.4 \times 10^{-7}$ | 0.0570 |
|  | 10 | 52,299,300 | $1.4 \times 10^{-8}$ | 0.0410 |
|  | 11 | 40,301,100 | $1.4 \times 10^{-9}$ | 0.0316 |
|  | 12 | 28,454,000 | $1.4 \times 10^{-10}$ | 0.0223 |
|  | 13 | 34,751,700 | $1.4 \times 10^{-11}$ | 0.0272 |
|  | $\sum$ | ~$1.277 \times 10^9$ |  | ~1 |

Relaxation times are shifted to $T^* = 120\ °C$.

The plots are intended to simulate the experimental measurements shown in Figure 5(a–c) and are again shown on identical axes to illustrate the differences between the materials and aid comparison with the data of Figure 5(a–c).

## DISCUSSION

It is helpful to consider the various experimental conditions in terms of the Weissenberg numbers associated with strain-rate and the various relaxation times of the polymer. For

example, $Wi_d^{AF} = \tau_d^{AF} \dot{\varepsilon}$ is the Weissenberg number associated with the disengagement, or reptation time $\tau_d^{AF}$ of polymer AF subjected to a strain rate $\dot{\varepsilon}$. As the samples were melt stretched at constant crosshead extension corresponding to a nominal strain rate $\dot{\varepsilon}_{nom}$, the true strain rate $\dot{\varepsilon}_{true}$ is changing during stretching and is given by $\dot{\varepsilon}_{true} = \dot{\varepsilon}/\lambda$. In the

**TABLE 4** Parameters for the Bond-Stretch Part of the Constitutive Model, Applicable to all Materials

| Parameter | Value | Source |
|---|---|---|
| $V_s$ (m$^3$/mol) | $2.6 \times 10^{-3}$ | Ref. 13 |
| $V_p$ (m$^3$/mol) | $0.24 \times 10^{-3}$ | Ref. 13 |
| $\Delta H$ (kJ/mol) | 113.6 | This work |
| $C$ (K) | 283.5 | This work |
| $T_\infty$ (°C) | 85.0 | This work |
| $T_{f,0}$ (redraw) (°C) | 98.9 | This work |
| $\Delta T_f$ (redraw) (°C) | 1.8 | This work |
| $\varepsilon_0^v$ (redraw) | 0.028 | This work |
| $G_b$ (GPa) | 1.28 | This work |
| $K$ (GPa) | 4.10 | Ref. 13 |

**TABLE 5** Parameters for the RP Part of the Constitutive Model

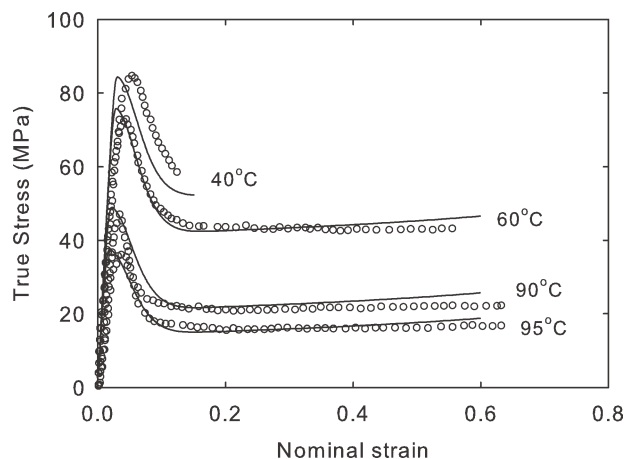|  | Parameter | Value | Source |
|---|---|---|---|
|  | $G_e$ (kPa) | 317.9 | This work |
|  | $M_e$ (kg/mol) | 13.14 | This work |
|  | $\tau_e$ at 120 °C (s) | 10.6 | This work |
|  | $\lambda_{max}$ | 4.09 | eq 14 |
| Polymer AF | $Z$ | 19.9 | This work |
|  | $\tau_1^R$ at 120 °C (s) | 4,203 | eq 12 |
|  | $\tau_1^d$ at 120 °C (s) | 165,620 | eq 13 |
| Polymer AG | $Z$ | 39.4 | This work |
|  | $\tau_1^R$ at 120 °C (s) | 16,430 | eq 12 |
|  | $\tau_1^d$ at 120 °C (s) | 1,400,000 | eq 13 |
| Polymer R | $Z$ | 16.4 | This work |
|  | $\tau_1^R$ at 120 °C (s) | 2,857 | eq 12 |
|  | $\tau_1^d$ at 120 °C (s) | 90,645 | eq 13 |

**FIGURE 7** Experimental measurements of uniaxial compression of isotropic specimens of polymer R at a range of temperatures from 40 °C to 95 °C at a rate of $\dot{\varepsilon} = 0.001\,\text{s}^{-1}$ from ref. 13 and constitutive model simulations for the same conditions.

time of one entanglement length ($Wi_e$) are defined similarly in terms of the corresponding relaxation times $\tau_R$ and $\tau_e$. A Weissenberg number much greater than unity indicates that relaxation does not occur during stretching, on the length scale associated with the corresponding relaxation time.
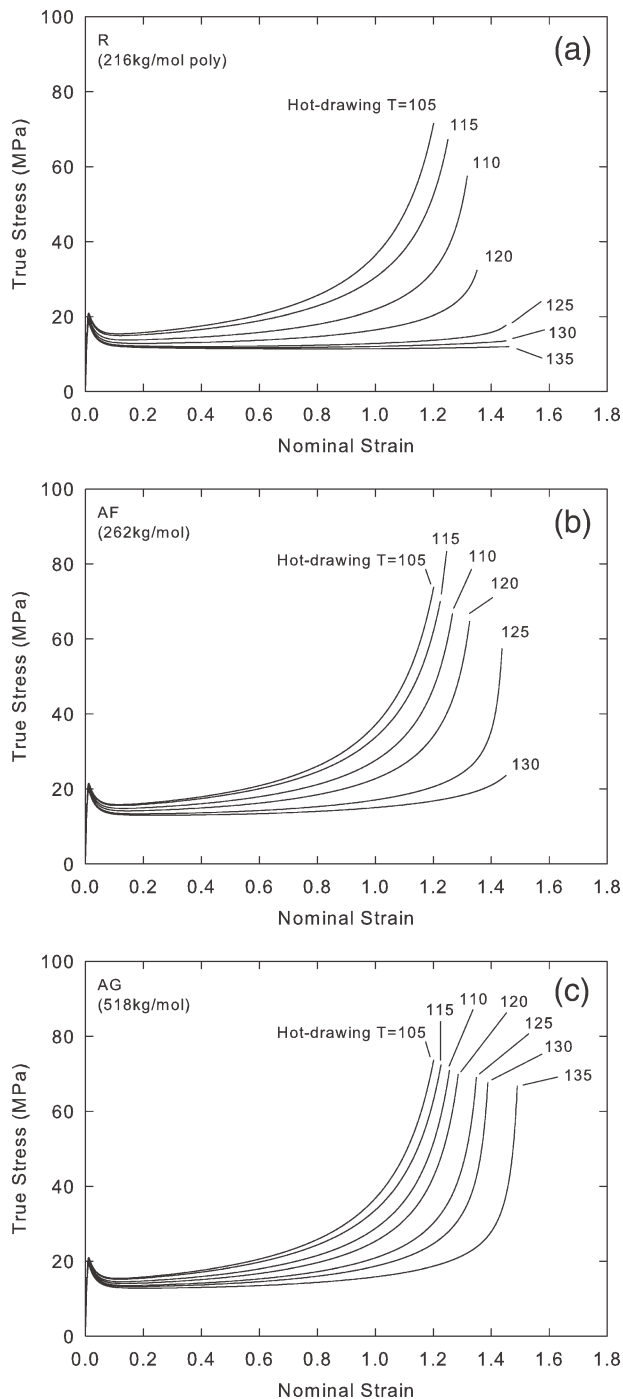


calculation of Weissenberg numbers used here, the nominal strain rate (equal to the true strain rate only at the beginning of melt stretching) is used. Weissenberg numbers associated with the longest Rouse time ($Wi_R$) and with the Rouse
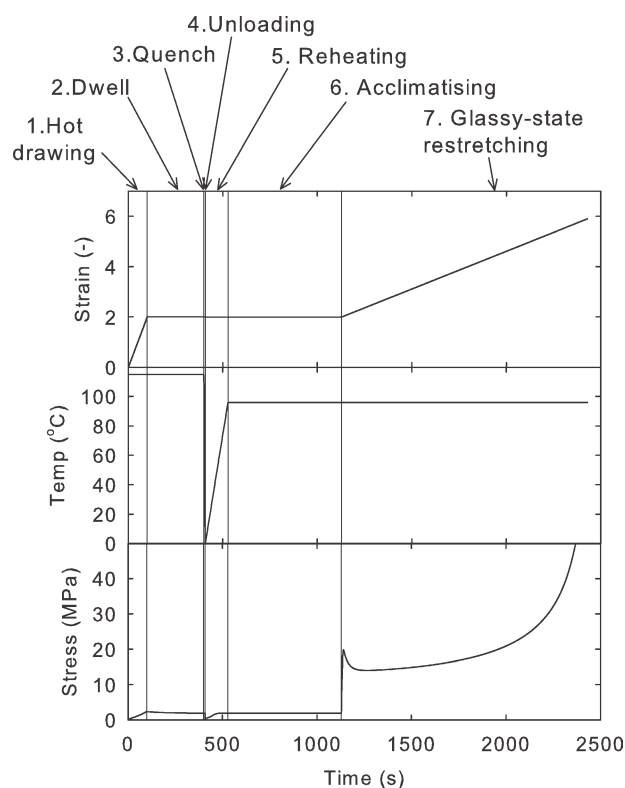


**FIGURE 8** Complete constitutive model simulation of the melt stretching process followed by a dwell time, quenching, unloading, reheating, acclimatizing, and restretching. Test parameters are for polymer AG drawn according to procedure III, at $T = 115$ °C, to $\lambda = 3$, followed by a 300 s dwell time before glassy-state uniaxial testing ($T_r = 96$ °C, $\dot{\varepsilon} = 0.001\,\text{s}^{-1}$).

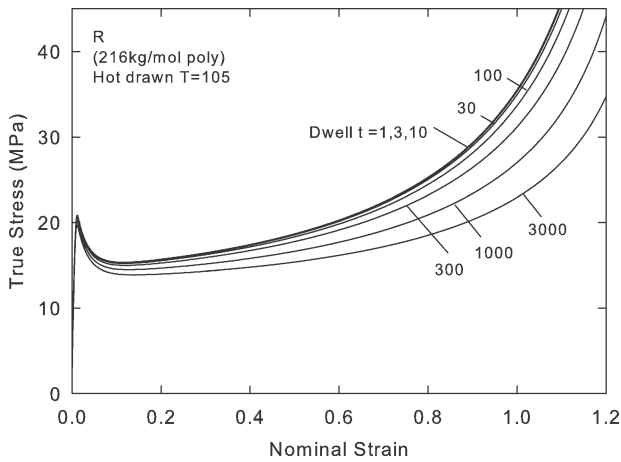**FIGURE 9** Constitutive model simulations of glassy-state uniaxial testing ($T_r = 96$ °C, $\dot{\varepsilon} = 0.001\,\text{s}^{-1}$) of material melt stretched according to procedure I, at a range of temperatures $T = 105$ °C–135 °C followed by immediate quenching, for materials R (a), AF (b), and AG (c).

**FIGURE 10** Constitutive model simulations of glassy-state uniaxial testing ($T_r = 96$ °C, $\dot{\varepsilon} = 0.001\,\mathrm{s}^{-1}$) of polymer R material melt stretched according to procedure II, at draw temperature $T = 105$ °C followed by a range of dwell times $t$ before quenching.

Figure 2 shows the application of the model to nonlinear viscoelastic rheology of material AG deep in the melt state, measured at 170 °C at a range of rates from 0.01 s$^{-1}$ to 10 s$^{-1}$, corresponding to $Wi_e \ll 1$. In effect, this shows the performance of the RP part of the model in isolation, since the bond-stretch arm of the model is fully relaxed. As expected, the model captures all of the trends visible in the experimental data and is quantitatively reasonably accurate over the full range of conditions. It is noteworthy that the nonlinear features of the RP part of the model visible in Figure 2 were not fitted to the data, but arise naturally from the molecularly based model.

In Figure 7, we consider the application of the model to the behavior of polymer R deep in the glassy state. Here, $Wi_R \gg 1$ and $Wi_d \gg 1$ over all the experimental data range. The simulations illustrate the performance of the bond-stretch part of the model in isolation. No relaxation occurs in the RP part of the model under these conditions, and the conformational stresses contribute a very small proportion of the total stress. Again, unsurprisingly, the model is able to capture adequately the yield peak and subsequent yield drop, and also qualitatively predicts the temperature dependence of the flow stress following yield relatively well, as was demonstrated previously.[13]

The simulations present in Figures 9–11 apply the model to the much more challenging cases of drawing in the glassy state following stretching in the melt. Figure 9 shows the consequences of melt stretching according to Procedure I. Here, the melt stretching was simulated at a rate and a range of temperatures specifically designed to cut across the fundamental relaxation times as much as possible. For instance, whereas the lowest melt stretch temperature of 105 °C corresponds to $Wi_e \approx 100$, the highest melt stretch temperature of 135 °C corresponds to $Wi_e \ll 1$ and $Wi_R^R = 0.9$, $Wi_R^{AF} = 1.3$ and $Wi_R^{AG} = 5.3$. Hence, during melt stretching, the processes of chain re-

traction and reptation are increasingly active as the temperature rises. Glassy-state drawing is simulated at $Wi_e \gg 1$. The results capture qualitatively all the important features of the stress–strain curves seen in the experimental data in Figure 3: a rise in yield stress and an earlier onset of strain hardening
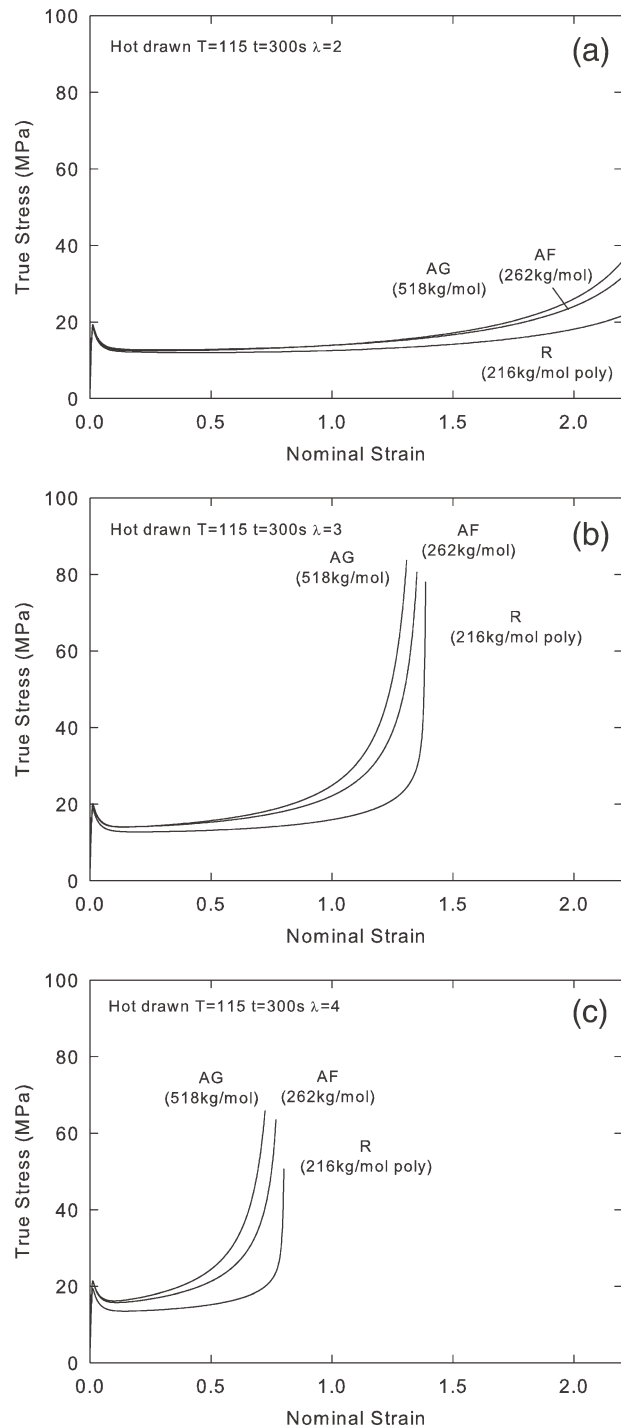


**FIGURE 11** True stress plotted against nominal strain measured during glassy-state uniaxial testing ($T_r = 96$ °C, $\dot{\varepsilon} = 0.001\,\mathrm{s}^{-1}$) of bars melt stretched according to procedure III, at a temperature of $T = 115$ °C followed by a dwell time of 300 s before quenching, for draw ratios $\lambda = 2$ (a), $\lambda = 3$ (b), and $\lambda = 4$ (c).

with decreasing melt stretch temperature. Quantitatively, however, the simulations become increasingly less accurate as the draw temperature is decreased. At lower draw temperatures, the onset of strain hardening occurs much earlier in the experimental data than in the simulations, and stresses are underestimated by the model. This suggests a contribution to the orientation arises from length-scales shorter than are represented in the constitutive model.

In the simulations of Figure 10, the model is applied to polymer R oriented at a temperature of $T = 105$ °C, followed by a varying dwell time before freezing. The simulated "melt stretch" here actually occurs at $Wi_e \gg 1$. The experimental data of Figure 4 illustrate that even short dwell times of a few seconds lead to visible delay in the onset of strain hardening. This is further evidence for the presence of a relaxation process affecting the flow stress and the onset of strain hardening whose associated timescale is less than $\tau_e$. This means that the length scale associated with this process is shorter than an entanglement length. The constitutive model simulations, on the other hand, become increasingly similar for dwell times less than 100 s. This is because within the model, there are no processes that recognize orientation below a timescale of $\sim\tau_e$, since all modes with associated length scales shorter than an entanglement are modeled in terms of an intrinsically isotropic viscoelastic process.

The simulations of Figure 11 explore the effect of varying the degree of stretch in melt stretching at $T = 115$ °C followed by 300 s dwell time before quenching. Here, the fundamental relaxation times are $\tau_e = 65$ s, $\tau_R^R = 17,700$ s, $\tau_R^{AF} = 26,000$ s, and $\tau_R^{AG} = 101,600$ s. The dwell time is $\sim$5 $\tau_e$, so in this case, one would not expect subentanglement processes with relaxation times shorter than $\tau_e$ to retain much orientation from the melt stretching history.

When compared with the experiments of Figure 5, the model simulations can be seen to be qualitatively correct, exhibiting all the major features of the experimental data: only small changes in yield stress, increase in strain-hardening with molecular weight, and a substantially earlier onset of strain-hardening with increasing degree of melt stretch. A quantitative comparison, however, reveals that, with increasing strain, the experimental data exhibit larger stresses than those seen in the simulations, across the range of conditions.

In summary, the new constitutive model gives good quantitative agreement with measurements on isotropic materials deep in the glassy state and deep in the melt state. This is no great surprise since it combines two models previously shown to perform well under these conditions. The present results show it is also able to capture qualitatively all of the features seen in glassy-state drawing of melt stretched polystyrene. Agreement here extends to the effects of melt stretch temperature, the degree of stretch, and polymer molecular weight. Quantitative shortcomings of the model are most evident in experiments where stretch of sub-entanglement length scales is taking place. Another feature of the results that can help shed light on this is the yield stress of oriented glassy polystyrene.

The effect of molecular weight on compressive yield stress in isotropic monodisperse PS was investigated by Wu and Buckley.[13] They measured an experimental rate of change of yield stress with $1/M_n$ to be $R_y = 3.1 \pm 1.2 \times 10^5$ MPa g mol$^{-1}$. They accounted for this by consideration of the effect of chain ends on the Vogel temperature and presented a quantitative means to incorporate this in a constitutive model, which, for the sake of simplicity, was not included in the simulations of this article.

In our experiments on oriented PS, the effects of molecular weight on yield stress manifest themselves through two distinct mechanisms: (A) a change in the number density of chain ends, leading to a change in the Vogel temperature, and hence the structural relaxation times, as pointed out by Wu and Buckley; and (B) a change in the length of chains, and hence in the conformational relaxation times associated with those lengths. In our materials, Wu and Buckley's measurement of $R_y$ accounts for a difference in isotropic yield stress of $2.4 \pm 0.9$ MPa between materials R and AF and of $3.0 \pm 1.1$ MPa between materials R and AG. We wish to isolate the effects of process (B) from the chain end density effects. To do this, for each of our experimental measurements in Figure 3, we calculate the value of an effective yield stress corresponding to an equivalent polymer with no chain ends, $\sigma_{y,\infty}$, from

$$\sigma_{y,\infty} = \sigma_y + \frac{R_y}{M_n} \qquad (19)$$

Figure 12 shows values of $\sigma_{y,\infty}$ computed from the data of Figure 3, plotted versus $Wi_e$. In the region where $Wi_e < 1$, all the materials exhibit a drop-off in yield stress with decreasing orientation, measured by $Wi_e$. The origin of this is a gradual relaxation of the conformational stress, reflecting molecular orientation that relaxes through reptation. This
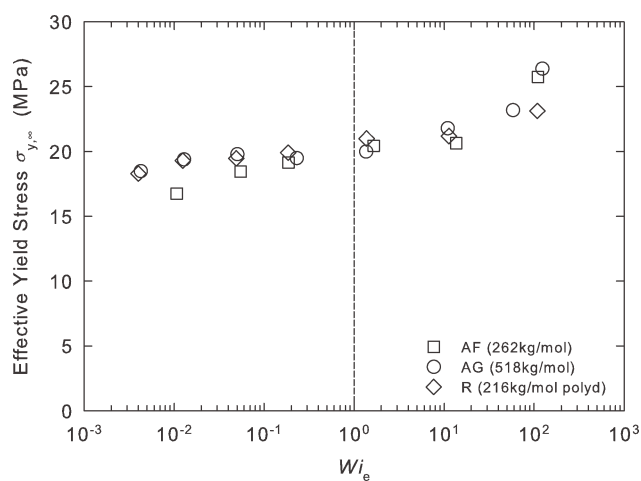


**FIGURE 12** Effective yield stress as computed from eq 19 of oriented material from polymers AF, AG, and R melt stretched according to procedure I, preoriented at temperatures from 105 °C to 135 °C at a strain rate of 0.02 s$^{-1}$ and immediately frozen, as a function of the $\tau_e$-based Weissenberg number.

is consistent with the structure of the constitutive model, whose longest conformational relaxation time is the reptation time of the polymer and whose shortest relaxation time is associated with the entanglement length scale.

The ROLIEPOLY part of the model is coupled in parallel with the bond-stretch part, such that the conformational stress makes a contribution to the yield stress. When $Wi_e$ exceeds unity, however, the effective yield stress measurements exhibit a substantial increase with increasing $Wi_e$ that appears approximately independent of molecular weight. This must reflect orientation occurring on a sub-entanglement length scale ($Wi_e > 1$), previously observed experimentally on PMMA by Wendlandt et al. using solid-state NMR[46] and by Casas et al. using neutron scattering.[47] It is further evidence that sub-entanglement orientation leads to more anisotropy of yield than is accounted for just by the conformational stress. The constitutive model does not at present capture this phenomenon. This is not surprising since in the model all modes corresponding to length scales shorter than an entanglement are modeled in terms of an intrinsically isotropic viscoelastic process, with no recognition of sub-entanglement orientation.

A clear message emerges from this accumulated evidence. The new model is successful in capturing the effects of molecular orientation induced in the melt on length-scales greater than an entanglement. It fails quantitatively when prior stretching involves shorter length-scales. This probably reflects the contribution from a further phenomenon (labeled process II earlier in this paper) that causes other discrepancies between the current model and experiment when applied deep in the glassy state, such as the recorded strain rate and temperature effects on the apparent strain hardening.[18,20,21] It is clear that orientation of molecular segments on a sub-entanglement length scale must also contribute to the development of anisotropy in the glassy state, but this is not yet recognized in the current model. A suggestion for how this could be done by recognizing the bond-stretch viscoelasticity as being intrinsically anisotropic has been proposed by Buckley.[22] Another approach to capturing this effect in a glassy-state constitutive model was suggested by Wendlandt et al., who introduced an empirical variation of Eyring activation volume with strain.[20] A physically based constitutive model that accounts fully for the stretching of subentanglement Rouse modes is currently lacking.

Another means of testing the ability of the current model to predict molecular orientation resulting from melt stretching is to compare its prediction of frozen-in optical birefringence with experimental measurements. Such a study was carried out by the authors as part of the present project and results will be reported elsewhere.

## CONCLUSIONS

A systematic experimental study has been made of the effects of molecular orientation on glassy-state viscoplastic deformation in atactic polystyrene, in which the roles of molecular weight, and parameters of the melt stretching history have been examined. The data have been compared with predictions made with a new framework for constitutive modeling of processed oriented polymers based on parallel coupling of two existing melt state and glassy-state models. The new combined glass-melt model is parameterized through its full linear viscoelastic spectrum, known molecular parameters of polystyrene, and additional parameters needed for capturing viscoplastic deformation of a glass.

When the model is assessed against results of nonlinear rheological experiments in the melt and uniaxial compression experiments deep in the glassy state, it is found to be quantitatively successful in capturing the material rheology. The model can also simulate the effects of processing conditions on frozen-in orientation, and its effects on polymer response in subsequent large deformations in the glassy-state. The model captures qualitatively all of the features seen in the experimental results, and also has the advantage of a molecular basis for the prediction of orientation. There are, however, quantitative shortcomings in the current model's predictions. These are predominant when the time–temperature conditions of melt stretching lead to molecular orientation on a sub-entanglement length-scale, since the model presented here contains no representation of intrinsic anisotropy on this length-scale.

## REFERENCES AND NOTES

**1** Ward, I. M. Structure and Properties of Oriented Polymers; Chapman & Hall: London, UK, 1977.

**2** Wright, H.; Faraday, C. S. N.; White, E. F. T.; Treloar, L. R. G. J Phys D Appl Phys 1971, 4, 2002–2014.

**3** De Francesco, A.; Duckett, R. A. Polymer 2004, 45, 8005–8011.

**4** Biswas, P. K.; Sengupta, S.; Basu, A. N. Colloid Polym Sci 1988, 266, 501–508.

**5** Broutman, L. J.; Mcgarry, F. J. J Appl Polym Sci 1965, 9, 609–626.

**6** Retting, W. Colloid Polym Sci 1979, 257, 689–710.

**7** Curtis, J. W. J Phys D Appl Phys 1970, 3, 1413–1422.

**8** Gotham, K. V.; Scrutton, I. N. Polymer 1978, 19, 341–347.

**9** Embery, J.; Graham, R. S.; Duckett, R. A.; Groves, D.; Collis, M.; Mackley, M. R.; McLeish, T. C. B. J Polym Sci Part B: Polym Phys 2007, 45, 377–394.

**10** Haward, R. N.; Thackray, G. Proc R Soc Lond A Math Phys Sci 1968, 302, 453–472.

**11** Buckley, C. P.; Jones, D. C. Polymer 1995, 36, 3301–3312.

**12** Buckley, C. P.; Dooling, P. J.; Harding, J.; Ruiz, C. J Mech Phys Solids 2004, 52, 2355–2377.

**13** Wu, J. J.; Buckley, C. P. J Polym Sci Part B: Polym Phys 2004, 42, 2027–2040.

**14** Boyce, M. C.; Parks, D. M.; Argon, A. S. Mech Mater 1988, 7, 15–33.

**15** Arruda, E. M.; Boyce, M. C.; Jayachandran, R. Mech Mater 1995, 19, 193–212.

**16** Tervoort, T. A.; Smit, R. J. M.; Brekelmans, W. A. M.; Govaert, L. E. Mech Time Dependent Mater 1998, 1, 269–291.

**17** Tervoort, T. A.; Govaert, L. E. J Rheol 2000, 44, 1263–1277.

**18** Govaert, L. E.; Tervoort, T. A. J Polym Sci Part B: Polym Phys 2004, 42, 2041–2049.

**19** Govaert, L. E.; Engels, T. A. P.; Wendlandt, M.; Tervoort, T. A.; Suter, U. W. J Polym Sci Part B: Polym Phys 2008, 46, 2475–2481.

**20** Wendlandt, M.; Tervoort, T. A.; Suter, U. W. Polymer 2005, 46, 11786–11797.

**21** Haward, R. N. Macromolecules 1993, 26, 5860–5869.

**22** Buckley, C. P. Presented at the 13th International Conference on Deformation, Yield and Fracture of Polymers, Kerkrade, The Netherlands, April 10–13, 2006.

**23** Dooling, P. J.; Buckley, C. P.; Rostami, S.; Zahlan, N. Polymer 2002, 43, 2451–2465.

**24** Palm, G.; Dupaix, R. B.; Castro, J. J Eng Mater Technol 2006, 128, 559–563.

**25** Adams, A. M.; Buckley, C. P.; Jones, D. P. Polymer 2000, 42, 771–786.

**26** Boyce, M. C.; Socrate, S.; Llana, P. G. Polymer 2000, 41, 2183–2201.

**27** Graham, R. S.; Likhtman, A. E.; McLeish, T. C. B. J Rheol 2003, 47, 1171–1200.

**28** Likhtman, A. E.; Graham, R. S. 2003, 114, 1–12.

**29** Bishko, G. B.; Harlen, O. G.; McLeish, T. C. B.; Nicholson, T. M. J Nonnewton Fluid Mech 1999, 82, 255–273.

**30** Lee, K.; Mackley, M. R.; McLeish, T. C. B.; Nicholson, T. M.; Harlen, O. G. J Rheol 2001, 45, 1261–1277.

**31** Bent, J.; Hutchings, L. R.; Richards, R. W.; Gough, T.; Spares, R.; Coates, P. D.; Grillo, I.; Harlen, O. G.; Read, D. J.; Graham, R. S.; Likhtman, A. E.; Groves, D. J.; Nicholson, T. M.; McLeish, T. C. B. Science 2003, 301, 2691–1695.

**32** Collis, M. W.; Lele, A. K.; Mackley, M. R.; Graham, R. S.; Groves, D. J.; Likhtman, A. E.; Nicholson, T. M.; Harlen, O. G.; McLeish, T. C. B.; Hutchings, L. R.; Fernyhough, C. M.; Young, R. N. J Rheol 2005, 49, 501–522.

**33** De Focatiis, D. S. A.; Buckley, C. P. Polym Test 2008, 27, 136–145.

**34** De Focatiis, D. S. A.; Buckley, C. P.; Hutchings, L. R. Macromolecules 2008, 41, 4484–4491.

**35** Likhtman, A. E.; McLeish, T. C. B. Macromolecules 2002, 35, 6332–6343.

**36** Sentmanat, M. L. Rheol Acta 2004, 43, 657–669.

**37** Figiel, Ł.; Dunne, F. P. E.; Buckley, C. P. Modell Simul Mater Sci Eng 2009, 18, 21.

**38** Cohen, A. Rheol Acta 1991, 30, 270–273.

**39** Note that in our modeling approach, the hydrostatic component of the stress is handled separately and linearly, see eq 2, and hence, we require the full component of each ROLIEPOLY stress $\sigma_k^c$ to be zero with no applied load. That is why we subtract the identity tensor from $T_k$ in eq 11 before multiplication with $G_e$. Also, since we are attributing only the deviatoric part of the stress to the RP terms, for each mode, $S_k^c$ is taken to be the deviatoric part of $\sigma_k^c$.

**40** Available at: http://www.reptate.com/, downloaded on 16/11/2009.

**41** Likhtman, A. E.; Milner, S. T.; McLeish, T. C. B. Phys Rev Lett 2000, 85, 4550–4553.

**42** It has been recognized in the literature that although $c_v = 1$ can produce marginally more precise fits to the linear rheological experimental data, a value of $c_v = 0.1$ is more consistent with nonlinear rheology and generally thought to be more realistic. The parameter is connected with convective constraint release, a mechanism which is not dominant in the linear regime. For our purposes, the main consequence of a change in $c_v$ is in the value of $M_e$ that is obtained from the optimization. For example, a value of $c_v = 0.1$ leads to parameters $G_e = 318$ kPa, $M_e = 13.1$ kg/mol, and $\tau_e = 0.000714$ s at the reference temperature $T^* = 170\ ^\circ$C. The quality of the fit to the linear data is marginally worse. A change in the value of $M_e$ subsequently leads to a change in the value of $\lambda_{max}$ through eq 14. We are not in a position to be able to use the present experimental data to identify the correct value of $\lambda_{max}$, and hence indirectly of $M_e$ and $c_v$, and therefore, we proceed with $c_v = 1$.

**43** Wagner, M. Korea-Aust Rheol J 2006, 18, 199–207.

**44** Brandrup, J.; Immergut, E. H.; Grulke, E. A. Polymer Handbook; Wiley: New York, 1999.

**45** Flory, P. J. Statistical Mechanics of Chain Molecules; Hanser Publishers: Munich, 1969.

**46** Wendlandt, M.; Tervoort, T. A.; van Beek, J. D.; Suter, U. W. J Mech Phys Solids 2006, 54, 589–610.

**47** Casas, F.; Alba-Simionesco, C.; Montes, H.; Lequeux, F. Macromolecules 2008, 41, 860–865.